

Interlayer tunneling spectroscopy and doping-dependent energy-gap structure of the trilayer superconductor $\text{Bi}_2\text{Sr}_2\text{Ca}_2\text{Cu}_3\text{O}_{10+\delta}$

Yoshiharu Yamada,¹ Kenkichi Anagawa,¹ Takasada Shibauchi,¹ Takenori Fujii,^{2,*} Takao Watanabe,^{3,†} Azusa Matsuda,^{3,2} and Minoru Suzuki^{1,‡}

¹*Department of Electronic Science and Engineering, Kyoto University, Kyoto 606-8501, Japan*

²*Department of Applied Physics, Faculty of Science, Tokyo University of Science, Tokyo 162-8601, Japan*

³*NTT Basic Research Laboratories, Nippon Telegraph and Telephone Corporation, 3-1 Morinosato-Wakamiya, Atsugi, Kanagawa 243-0198, Japan*

(Received 7 December 2002; revised manuscript received 19 May 2003; published 29 August 2003)

The superconducting gap, the pseudogap, and their doping and temperature dependences have been measured by the short-pulse interlayer tunneling spectroscopy for the CuO_2 triple-layer high- T_c superconducting $\text{Bi}_2\text{Sr}_2\text{Ca}_2\text{Cu}_3\text{O}_{10+\delta}$ system. It is found for a nearly optimally doped sample that the superconducting gap magnitude is ≈ 80 meV and the pseudogap is ≈ 120 meV, the values of which are slightly larger than those for CuO_2 double-layer system. Both gap magnitudes show a clear tendency to decrease with increasing doping. In an underdoped sample, a clear dip-and-hump structure is observed, which declines with increasing doping and tends to diminish in overdoped samples. The relationship between unchanged T_c and decreasing superconducting gap in the overdoped region is discussed in terms of the proximity effect applied to the inequivalent doping model. We also discuss the dip-and-hump structure in comparison with other spectroscopic results. Finally, we argue an important implication of the increasing maximum Josephson current and the decreasing superconducting gap magnitude, both with increasing doping.

DOI: 10.1103/PhysRevB.68.054533

PACS number(s): 74.72.Hs, 74.50.+r, 74.25.Jb

I. INTRODUCTION

Tunneling spectroscopy directly probes the electronic structure of a metal that composes a tunnel junction.¹ When the metal is in the superconducting state, this technique vividly traces the evolution of the superconducting gap. After the discovery of the high- T_c superconductivity,² two types of tunneling spectroscopy techniques were newly or renewedly developed. One is the scanning tunneling spectroscopy (STS)^{3,4} and the other is the interlayer tunneling spectroscopy (ITS).^{5,6} While the former stemmed from the original work of Binnig and Rohrer⁷ on the scanning tunneling microscope, the latter utilizes naturally built tunnel junctions in a layered crystal structure, commonly called intrinsic Josephson junctions.^{8,9} As is well known, STS probes a surface on an atomic scale. After its precedent application to the observation of a vortex core in NbSe_2 (Refs. 10 and 11), STS was applied to high- T_c superconductors to reveal the superconducting energy-gap structure,^{4,12-15} electronic states in vortex structure,¹⁶ and, very recently, local electronic inhomogeneity (at least at surfaces) with an atomic scale resolution.¹⁷⁻²⁰ This technique is applicable to almost any kind of conducting material as far as a clean surface is available. On the other hand, ITS is essentially a technique probing into the bulk (not the surface) of a layer-structured material. Therefore, this technique is free from surface problems that disguise the intrinsic properties. It is an advantage of this technique that the probed part can be characterized simultaneously by transport measurements, providing a solid basis for the sample that yielded the results. However, this method relies on tunnel junctions in a crystal structure and is applicable only to a limited number of layered materials, in which layers are coupled via tunneling. Although ITS has

provided important results, the materials employed were limited mostly to $\text{Bi}_2\text{Sr}_2\text{CaCu}_2\text{O}_{8+\delta}$, a CuO_2 double-layer high- T_c superconductor,^{5,6,21-24} except $\text{Tl}_2\text{Ba}_2\text{Ca}_2\text{Cu}_3\text{O}_{10+\delta}$, in which the range observed was limited far below the superconducting gap.²⁵

This paper reports the results of the ITS experiment on a CuO_2 trilayer high- T_c superconductor $\text{Bi}_2\text{Sr}_2\text{Ca}_2\text{Cu}_3\text{O}_{10+\delta}$ (Bi2223). The basis for the present ITS experiments was initiated by the first single-crystal growth of Bi2223 by the traveling-solvent-floating-zone method.²⁶ Bi2223 is crystallographically equivalent to the $\text{Bi}_2\text{Sr}_2\text{CaCu}_2\text{O}_{8+\delta}$ (Bi2212) system when the CuO_2 double layer (bilayer) is replaced by the CuO_2 triple layer. The transport properties of the Bi2223 system were measured recently by Fujii *et al.*^{27,28} They revealed an anomalous carrier doping dependence, in which T_c remains fixed in the overdoped region irrespective of the doping level. This behavior is apparently at variance with the generic phase diagram,²⁹ which is accepted as a universal feature for the understanding of high- T_c superconductivity. At present, it is believed that this anomalous behavior is explained in terms of the inequivalent carrier doping,^{27,28} which takes place between two inequivalent CuO_2 layers in the triple-layer system. In such a system, the energy-gap structure and its relation to T_c or carrier doping are yet to be known. To reveal the existence of the pseudogap and its magnitude is also interesting as a key factor in the generic phase diagram. From such points of view, the knowledge of the electronic structure of this Bi2223 system is thought to deepen the understanding of high- T_c superconductivity.

The electronic structure of the Bi2223 system was recently measured by the angle-resolved photoemission spectroscopy (ARPES) by Feng *et al.*³⁰ and Sato *et al.*³¹ They made it clear that the superconducting energy gap Δ_{SG} for

each system scales with the optimum T_c in the corresponding system. The observed values for Δ_{SG} by both groups are similar, i.e., $\Delta_{SG}=45\text{--}55$ meV for an optimally doped sample, when they are evaluated from the superconducting peak (SCP) or $\Delta_{SG}=30\text{--}33$ meV from the leading edge midpoint (LEM) shift. The pseudogap was also observed by ARPES (Refs. 30 and 31) but much remains to be studied concerning its doping-dependent magnitude and the temperature T^* , below which the pseudogap evolves.

Along with the superconducting gap and pseudogap, the peak-dip-hump (PDH) structure³² is another source of interest associated with the electronic structure of high- T_c superconductors. This structure has been observed in Bi2212 by both ARPES³³ and tunneling spectroscopy.³⁴ Its origin is an issue and argued in various ways.^{32,35–37} The recent ARPES measurements revealed that PDH structure is observed in the Bi2223 system.^{30,31} Since ITS is free from the surface problem, the observation of the PDH structure by ITS may provide additional information to elucidate its origin.

In the present study, we have obtained the superconducting gap magnitude of $2\Delta_{SG}=79$ meV for the optimum doping level. This is found to be a little smaller than the ARPES value^{30,31} evaluated from the SCP position. The pseudogap magnitude $2\Delta_{PG}$ we observed is ≈ 130 meV, which is comparable with the value of $2\Delta_{PG}=100$ meV observed by Sato *et al.*, indicating rough coincidence between the ARPES results and the ITS results. Furthermore, the ITS measurements of the Bi2223 gap structure have been extended to samples from underdoped to overdoped levels to obtain doping-dependent behavior of the gap structures. It is found that the superconducting gap and the pseudogap magnitudes decrease with the doping level. We have also observed a systematic and profound change in the PDH structure, which is discussed in comparison with the corresponding structure in the spectral function observed in ARPES measurements.^{30,31}

Since a sample is a stack of intrinsic Josephson junctions, we also measured the maximum Josephson current at various doping levels to find that the maximum dc Josephson current increases significantly with the doping level. The doping dependences are reasonably compared with the doping-dependent transport properties observed by Fujii *et al.*^{27,28} The relevance of the doping independent T_c and the doping-dependent superconducting gap in the overdoped region is discussed in terms of the McMillan tunneling model of the proximity effect.³⁸ Finally, we discuss the implication of the doping-induced decrease in Δ_{SG} and the concomitant increase in the maximum Josephson current to deduce a decisively important nature of high- T_c superconductivity, at least in this system.

II. EXPERIMENT

A. Sample preparation

Samples used for the ITS measurements were prepared from single crystals grown by the traveling-solvent floating-zone method.²⁶ A sample for ITS consists of a small-sized mesa structure, which comprises ten or less intrinsic Josephson junctions connected in series; namely, the thickness of a

mesa is ≈ 19 nm in this case. The lateral size of a mesa is mostly $10\times 10\ \mu\text{m}^2$ for underdoped and slightly overdoped samples and $5\times 5\ \mu\text{m}^2$ for overdoped samples. Mesa structures were fabricated by engraving a cleaved crystal surface by the standard Ar-ion milling and photolithograph technique. Prior to these patterning and milling processes, the cleaved surfaces were covered with a 25-nm-thick Ag and a 50-nm-thick Au double layer, both for surface protection from damages and for formation of good electrical contact. After the Au/Ag film coating, the crystals were annealed at 430–450 °C in flowing oxygen or in vacuum depending on the required doping level. The doping level was controlled primarily by changing the annealing time. The condition to give underdoped samples is rather subtle. Strong reduction processes resulted in a high contact resistance and a low T_c with a broad resistive transition, which are not suitable for the ITS measurements. Therefore, we eventually attained only a single doping level in the underdoped region. Samples in the overdoped region were almost free from this kind of a problem. After the Ar-ion milling, a 350-nm-thick SiO insulating layer was deposited by the self-alignment method. A 450-nm Au upper electrode was finally deposited and patterned by the lift-off method. Thus, the total thickness of a Au/Ag film on top of the mesa amounts to 525 nm. This rather thick Au/Ag electrode is significantly important to suppress self-heating due to current injection during measurements. It is shown by the numerical analysis that more than half of the heat generated in the mesa flows out through the upper Au electrode channel.^{39,40} Therefore, we adopted the three-terminal configuration for the tunneling measurements at the expense of a finite contact resistance. A schematic cross-sectional illustration for the mesa structure is shown in the inset to Fig. 1.

The contact resistance for most of the samples ranged from 1 to 6 Ω [in contact resistivity, $(1\text{--}6)\times 10^{-6}\ \Omega\ \text{cm}^2$], which is approximately 1–10 % of the mesa resistance R_c at 300 K. The current-voltage (I - V) characteristics for samples having a larger contact resistance exhibit nonlinearity at small currents. At large currents for these samples, the voltage drop at the contact resistance does not increase proportionally to the current due to its nonlinearity so that the contact resistance becomes rather small at higher currents. Therefore, the tunneling characteristics for $I\gtrsim 10$ mA are subjected to little influence of the contact resistance, and hence, so is the gap magnitude. We estimate such effective contact resistance to be smaller than R_c by more than two orders of magnitude. For this reason, the contact resistance was neglected in the data analysis which follows.

The number of intrinsic Josephson junctions, N , included in the mesa was determined by observing I - V characteristics and counting the number of resistive branches. In the present study, N ranged from 8 to 10. These values for N roughly coincide with the mesa thickness estimated from the Ar-ion milling time. The mesa thickness was determined from N using a single-layer thickness value of 1.85 nm (Ref. 41), i.e., half the c -axis lattice parameter for the Bi2223 crystal structure. The mesa area was precisely determined by directly observing the mesa pattern with an optical microscope.

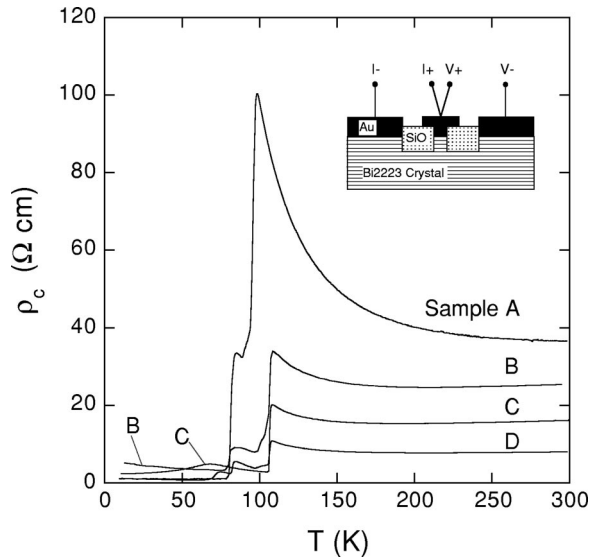


FIG. 1. Temperature dependence of ρ_c for samples having different doping levels. Excitation current is $1 \mu\text{A}$ for sample A and $5 \mu\text{A}$ for samples B–D. An additional resistive transition at about 80 K is caused by Bi2212 intergrowth. Residual resistance seen below 80 K is contact resistance. Samples B–D are differently doped, but undergo the resistive transition at nearly the same temperature of 107 K.

Using these dimensions for the mesa area and thickness, values for the c -axis resistivity ρ_c were determined.

B. Short-pulse measurements

ITS measurements were carried out by the short-pulse method. Employing short pulses is requisite to reduce the self-heating effect sufficiently. We used composite current sinusoidal curves both at the front and back of a rectangular pulse. This pulse shape was shown to be effective in increasing the breakdown voltage and eliminating sample breakage by fatigue.⁴² Voltage responses were acquired at 0.6–0.65 μs from the rise of the pulse. The voltage values were smoothed to give numerical differential (dI/dV)- V curves.

From the pulse response decay, it was known that the self-heating exerts an influence on the I - V characteristics when the current exceeds $\approx 25 \text{ mA}$ for a $10 \times 10\text{-}\mu\text{m}^2$ junction. At this current level, the voltage response was reduced in its magnitude by $\approx 3\%$ at the corresponding voltage in the I - V curve. For overdoped samples, this voltage roughly corresponds to the superconducting gap, in which case the gap magnitude is underestimated by $\approx 3\%$. However, this is not the case for samples which are nearly optimal or in the underdoped region, since the tunneling resistance R_N is sufficiently high and the gap voltage is reached at a current much smaller than 25 mA.

III. RESULTS

A. c -axis resistivity ρ_c

Figure 1 shows the temperature T dependence of ρ_c for four typical samples with different doping levels. Unlike the

case for the Bi2212 system,⁴³ the doping level, or oxygen content δ , is not determinable from $\rho_c(T)$, since the relationship between the doping level and the $\rho_c(T)$ curve is not fully established. However, the doping dependence of the transport properties by Fujii *et al.*^{27,28} shows that the value for ρ_c at 300 K is a good measure for the doping level; namely, ρ_c decreases systematically with increasing doping level,⁴⁴ as shown in Fig. 1. With decreasing doping level, the T dependence of ρ_c becomes pronouncedly semiconductive. This behavior of ρ_c is reasonably compared with the results for bulk single crystals reported by Fujii *et al.*^{27,28}

At the resistive transition, several samples exhibited a two-step resistive transition, first at 107 K and second at about 80 K. This two-step resistive transition is due to the intergrowth of Bi2212 layers.²⁶ When a single Bi2212 layer is included in a Bi2223 layer stack, two junctions out of, say, ten junctions are heterojunctions, which undergo a resistive transition at the Bi2212 transition temperature of 80 K. Therefore, the resistive transition at 107 K undergoes $\approx 80\%$ of the total resistive transition and at $\approx 80 \text{ K}$ it completes the rest of the transition. The resistive transition of sample A is compared with this case and it is reasonably concluded that sample A contains a single Bi2212 intergrowth layer. This result implies that the superconductivity of a different T_c sets in even in a single sheet of a CuO_2 double layer. The existence of a half unit-cell Bi2212 intergrowth was actually observed by the transmission electron microscopy.²⁶

Samples B–D in Fig. 1 exhibit a sharp resistive transition at 107 K, implying that they are located near the optimum doping level or in the overdoped region. For samples A, B, and D, it is seen that the mesa contains a single Bi2212 intergrowth layer. The energy-gap structure for the Bi2212 system is, strictly speaking, different from that of the Bi2223 system and the difference may be reflected on the tunneling spectroscopy results. However, its difference is reasonably considered to be small compared with the gap magnitude, and further the difference is divided by $N \sim 10$ at the normalization step in the analysis. Therefore, the influence of the Bi2212 intergrowth, if any, is estimated to be a few percent or less, so that the error due to the intergrowth is neglected⁴⁵ in the analysis which follows.

B. I - V characteristics

Figure 2 shows an oscilloscope image of typical I - V characteristics for a Bi2223 mesa of sample A, showing ten resistive branches. A closer look at Fig. 2 reveals asymmetry of the resistive branches. The reason for this is subtle. First, it must be noted that the graph is a multiscan trace. In a current scan, the order of switching to the voltage state for each junction varies from scan to scan. In addition, it frequently occurs that more than one junctions switch to the resistive state at a time. Such switching behavior together with a scatter in the Josephson current is thought to result in the asymmetry in the resistive branches.

As seen in this figure, there is a tendency that a few junctions have a smaller maximum Josephson current I_c . The reason for this is yet to be known but is conjectured to be partly due to a scatter of junction area among those in the

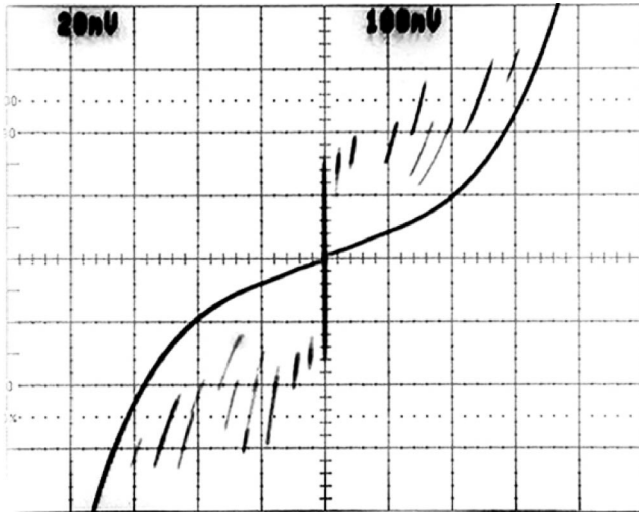


FIG. 2. An oscilloscope image of the I - V characteristics for sample A measured at 7 K. X axis, 100 mV/div; Y axis, 200 μ A/div. The number of junctions N for this sample is 10, as revealed by the number of resistive branches.

stack or it might be due to a vortex incorporated in the mesa structure. Taking these into account, I_c is determined to be the probable maximum current among resistive branches observed in the I - V characteristics. For the sample in Fig. 2, I_c is determined to be 0.6 mA. Values for other samples were determined similarly.

In the I - V curves in Fig. 2, the spacing between resistive branches for the lowest two appears to be smaller than the others. This is partly because the Josephson current is small and the spacing is reduced due to nonlinear quasiparticle current and partly because the mesa contains a single Bi2212 intergrowth layer, which may lead to a smaller spacing.

Figure 3 shows a set of typical I - V characteristics measured by the short-pulse method at various temperatures from 10 to 200 K. In the figure, the abscissa scale represents the normalized voltage for a single junction, i.e., the observed voltage divided by N . Above T_c , the pseudogap manifests itself as a nonlinearity in the I - V curves. In this set of I - V curves, it should be emphasized that, at high voltages at any temperatures, the I - V curve approaches the straight line that crosses the origin, the behavior of which is a consequence of a usual tunneling theory. The normal tunneling resistance R_N is defined as the static resistance at high voltages where the I - V curve sufficiently approaches the straight line that crosses the origin. These characteristics are in sharp contrast with the break junction characteristics,⁴⁶ where the I - V curve at high voltages deviates significantly from the straight line that crosses the origin. Such anomalous characteristics probably originate from break junction's undefined junction area, which might be a function of bias voltage, temperature, and others. It is also conjectured that self-heating causes this type of anomalous I - V characteristics in such junctions.

In the present case, the junction area S is unambiguously defined by the geometrical mesa size. Therefore, the I - V curve approaches the straight line at high voltages, as the standard tunneling theory predicts, providing definite values

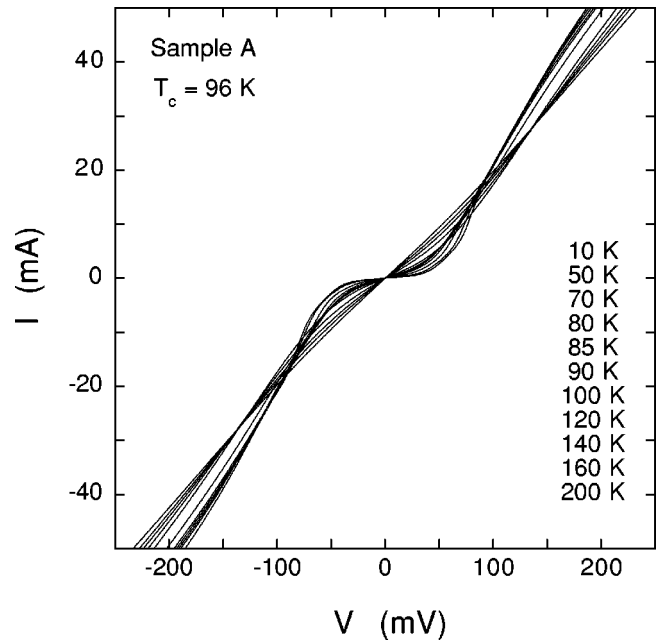


FIG. 3. I - V characteristics for sample A at different temperatures measured by the short-pulse method. V is the normalized voltage for a single junction.

for R_N . Values for the normalized tunneling resistance $\rho_N = R_N S/d$ are plotted in Fig. 4 for corresponding samples. From this, it is clearly seen that R_N increases with increasing T . This presents a sharp contrast with the semiconductive behavior exhibited by ρ_c , which is the dynamic resistance at $V=0$ in Fig. 2. The same behavior is observed in the Bi2212 system.⁶ It is also seen that ρ_N coincides with ρ_c in the T range where ρ_c shows metallic behavior. This is a plain consequence that the pseudogap is filled and vanishes in this T range, in which the I - V curve is straight. The stepwise decrease $\Delta\rho_N$ just below T_c is supposed to be related to the superconducting condensate.⁶ Its fractional magnitude $\Delta\rho_N/\rho_N$ depends on the doping level and increases with increasing doping, as demonstrated in Fig. 4. This is also closely related to the maximum Josephson current density J_c , as we will refer in the following section.

Definite evaluation of R_N is important when the Josephson current is discussed. Indeed, it turns out later that R_N and J_c are key factors that lead to an important consequence concerning the nature of high- T_c superconductivity in this system.

C. Tunneling spectrum

Figures 5(a)–5(c) show the dI/dV - V characteristics for samples at underdoped, nearly optimum, and overdoped levels, respectively. In these figures, the abscissa scale also indicates the normalized voltage. In these dI/dV - V characteristics, or differential tunneling conductance $\sigma_T(V)$, a sharp peak is clearly seen, which decreases in height and position with increasing T and disappears at T_c . Therefore, in the case of Fig. 5(a), the peak at 82 meV at 10 K is the superconducting peak. We define the superconducting gap magni-

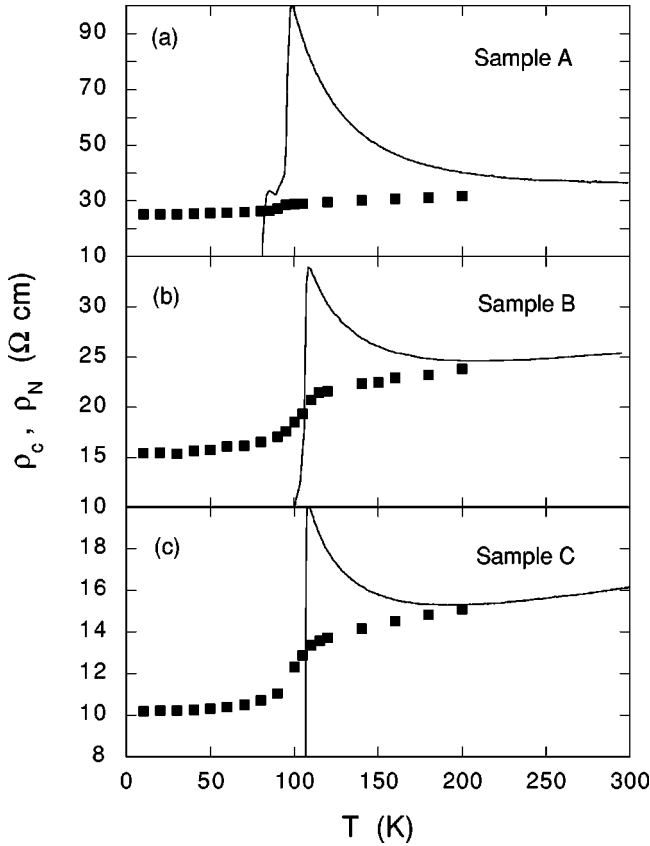


FIG. 4. Temperature dependence of the normal tunneling resistance R_N normalized by the dimensional factor S/d , i.e., $\rho_N = R_N S/d$ for samples A–C. ρ_N is compared with ρ_c to be found to approach ρ_c at high temperatures asymptotically. Plots are ρ_N and solid lines are ρ_c .

tude $2\Delta_{SG}$ as half the peak separation, so that $2\Delta_{SG} = 82$ meV for the underdoped sample of sample A.

For the nearly optimally doped and overdoped samples [samples B and C in Figs. 5(b) and 5(c)], $2\Delta_{SG} = 79$ meV and $2\Delta_{SG} = 64$ meV, respectively. The latter value is clearly smaller than that for the underdoped sample, indicating a tendency that $2\Delta_{SG}$ decreases with increasing doping level. Clearly, this decrease in $2\Delta_{SG}$ is not caused by the Bi2212 intergrowth, because the frequency of Bi2212 intergrowth is one part per ten or less and irrelevant to the doping. It is also clear that the height of the superconducting peak increases with increasing doping level. Even when the peak height is normalized by the value for $\sigma_T(0)$ at 200 K, it increases with increasing doping. This behavior is accompanied by an increase in the maximum Josephson current density J_c in the I - V characteristics. At first thought, it is conjectured that this is related to an increase in the superfluid density, which is expected to increase with doping. We discuss in the following section that this may not be the case.

In Fig. 5(a), besides the superconducting peak at 82 meV, another broad peak is seen at ≈ 120 meV. This peak also decreases in height with increasing T , becomes broader, and collapses to form a broad hump near and above T_c . This broad peak at 120 meV might be viewed as a hump of the PDH structure in the ARPES energy dispersion curve near

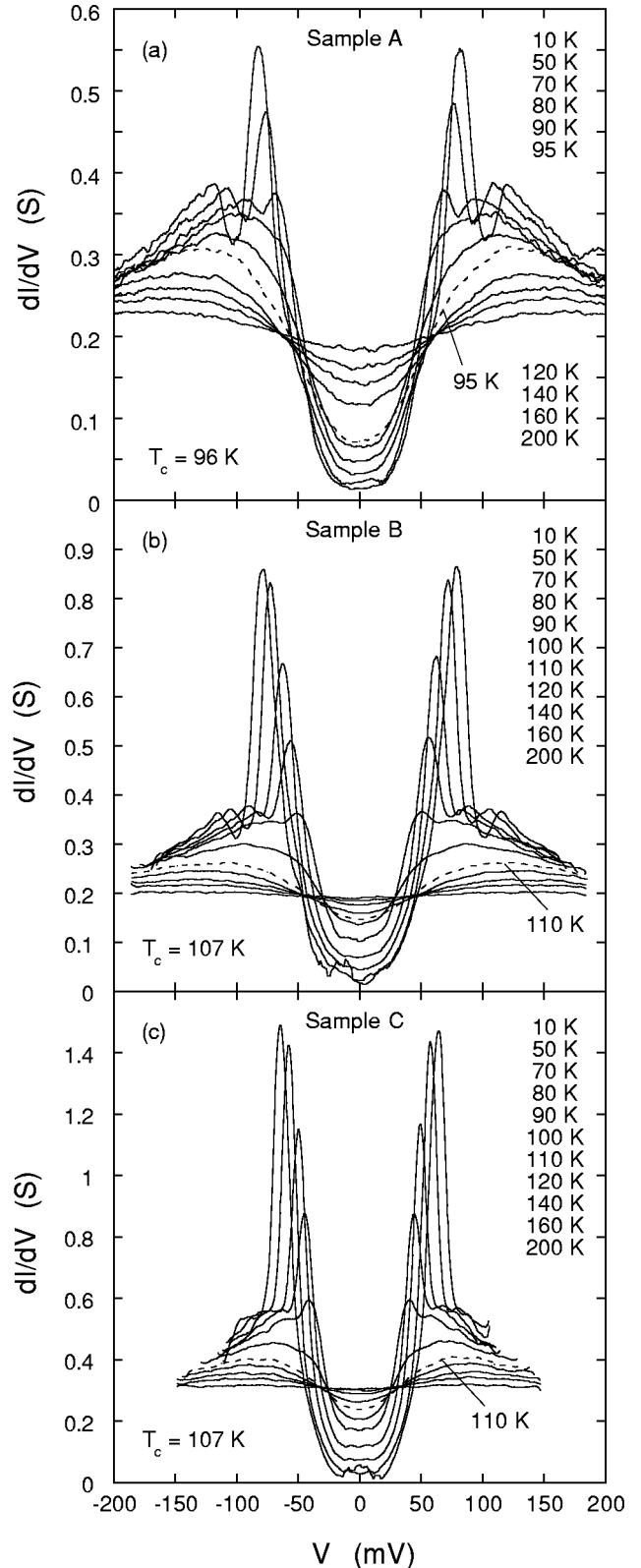


FIG. 5. (dI/dV) - V curves at various temperatures obtained numerically for samples A–C. The voltages are normalized by the junction number N . The dashed lines indicate the curves close to T_c for corresponding samples. The irregularities near $V=0$ are caused by the unsuppressed Josephson currents.

TABLE I. Values for Δ_{SG} , Δ_{PG} , N , T_c , R_c , ρ_c , R_N , contact resistance R_{contact} , and various properties, together with sample dimensions S and d for samples A–D.

Sample	A	B	C	D
T_c (K)	96	107	107	107
$2\Delta_{SG}$ (10 K) (meV)	82	79	65	53
$2\Delta_{PG}$ (150 K) (meV)	~ 150	~ 130	~ 90	~ 60
$2\Delta_{SG}/k_B T_c$	9.7	8.6	7.1	5.8
N	10	8	10	8
ρ_N (200 K) (Ω cm)	31.7	23.8	15.1	7.27
J_c (≤ 10 K) (A/cm^2)	470	1700	5100	7800
ρ_c (300 K) (Ω cm)	36.6	25.4	13.0	8.0
R_c (300 K) (Ω)	53.6	43.1	34.2	62.2
R_{contact} (~ 10 K) (Ω)	1.7	5.1	5.0	5.9 (at 64 K)
Mesa pattern (μm^2)	10×10	10×10	10×10	5×5
S (μm^2)	127	88	87	19
d (nm)	18.5	14.8	18.5	14.8

the $(\pi, 0)$ point. However, the structure in Fig. 5(a) is a broad peak rather than a hump, and its position is much lower than that in the ARPES results of 100 meV (Ref. 30) or higher,³¹ to which Δ_{SG} should be added when compared with the hump position in superconductor/insulator/superconductor (SIS) tunneling results, as discussed in the following section. At present, it does not necessarily follow straightforwardly that the peak at 120 meV in Fig. 5(a) directly conforms to the PDH structure in ARPES. The PDH structure becomes more significant for underdoped samples because of the relatively smaller height of the superconducting conductance peak. We should stress the fact that the PDH structure observed in the present study is very sharp and clear, in particular for sample A. This is partly due to the high resolution of SIS tunneling spectroscopy. It is also noteworthy that the background of $\sigma_T(V)$ evolves systematically as T decreases.

Above T_c , the tunneling conductance $\sigma_T(V)$ changes to a broad peak located at ≈ 120 meV for the underdoped sample [Fig. 5(a)]. This is clearly the pseudogap in the Bi2223 system. Here, we define the magnitude of the pseudogap $2\Delta_{PG}$ as half the peak separation. As the temperature is raised, the peak structure becomes obscure and the peak position shifts slightly to higher energies. When the peak is low and broad, $2\Delta_{PG}$ was determined by enlarging the portion vertically. In that case, a scatter of data eventually caused a large uncertainty in the value for $2\Delta_{PG}$. The obtained values for $2\Delta_{PG}$ at 150 K for samples A–C are 150 meV, 130 meV, and 90 meV, respectively. It is clear that $2\Delta_{PG}$ decreases with increasing doping in the Bi2223 system. Similar tendency was observed in the Bi2212 system.²¹ Values for Δ_{SG} and Δ_{PG} are summarized in Table I for samples A–D together with those for various properties and dimensions.

It appears that this pseudogap structure connects smoothly with the background below T_c , on which the superconducting gap and the dip structure are thought to evolve, or it may be that the pseudogap structure connects smoothly with the hump structure itself. If we regard the background to be re-

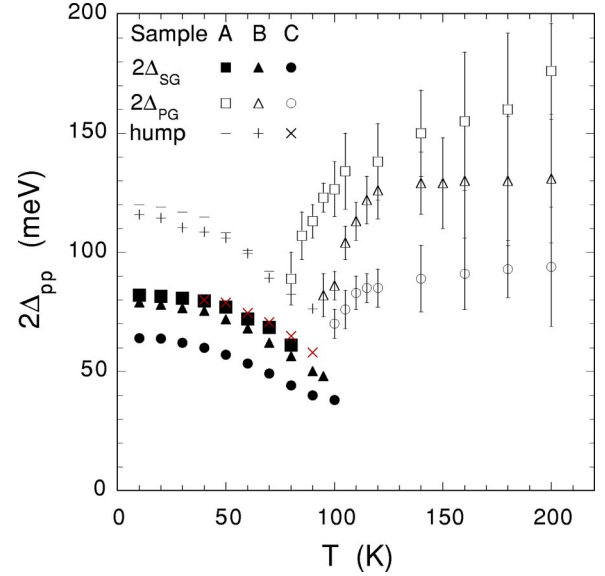


FIG. 6. Temperature dependence of half the peak separation $2\Delta_{pp}$ in (dI/dV) - V tunneling characteristics for samples A–C shown in Fig. 5. Plots for $T < T_c$ correspond to $2\Delta_{SG}$, while plots for $T > T_c$ correspond to $2\Delta_{PG}$. The hump positions are also plotted.

lated to the pseudogap, it naturally follows that the superconducting peak is distinct from the pseudogap. In the same sense, the superconducting gap does not directly connect with the pseudogap above T_c . This is also a consequence from the distinct T -dependent behavior of the superconducting gap, which swiftly diminishes in height and energy scale as T approaches T_c and finally disappears at T_c .

From Fig. 5, it is possible to estimate values for T^* , below which the pseudogap evolves. For the underdoped sample in Fig. 5(a), $\sigma_T(V)$ at 200 K shows a broad dip centered at $V=0$ so that T^* is much higher than 200 K. For the nearly optimum and slightly overdoped samples in Figs. 5(b) and 5(c), only a trace of broad dip is seen in $\sigma_T(V)$ at 200 K for both samples, indicating that $T^* \approx 200$ K for the optimum and slightly overdoped Bi2223 system. This result for T^* is in reasonable agreement with T^* obtained from the transport measurements by Fujii *et al.*^{27,28}

Figure 6 shows the temperature dependence of half the peak separation $2\Delta_{pp}$ and the hump positions in the $\sigma_T(V)$ curves. $2\Delta_{pp}$ represents $2\Delta_{SG}$ for $T < T_c$ and $2\Delta_{PG}$ for $T > T_c$. The temperature dependence for $2\Delta_{SG}$ is quite similar to that for the Bi2212 system. $2\Delta_{SG}$ decreases with increasing T and, above ≈ 90 K, the superconducting peak is almost indiscernible and Δ_{SG} is indeterminate in this range from 90 K to T_c . The peak in $\sigma_T(V)$ switches from the superconducting gap to the pseudogap at around 90 K, from which it appears that Δ_{pp} reaches the minimum at ~ 90 K, then increases with increasing T , and finally approaches the pseudogap value above T_c .

D. Doping dependences

Figure 7 shows the plots of values for T_c , the maximum Josephson current density J_c at low temperatures, $2\Delta_{SG}$, and

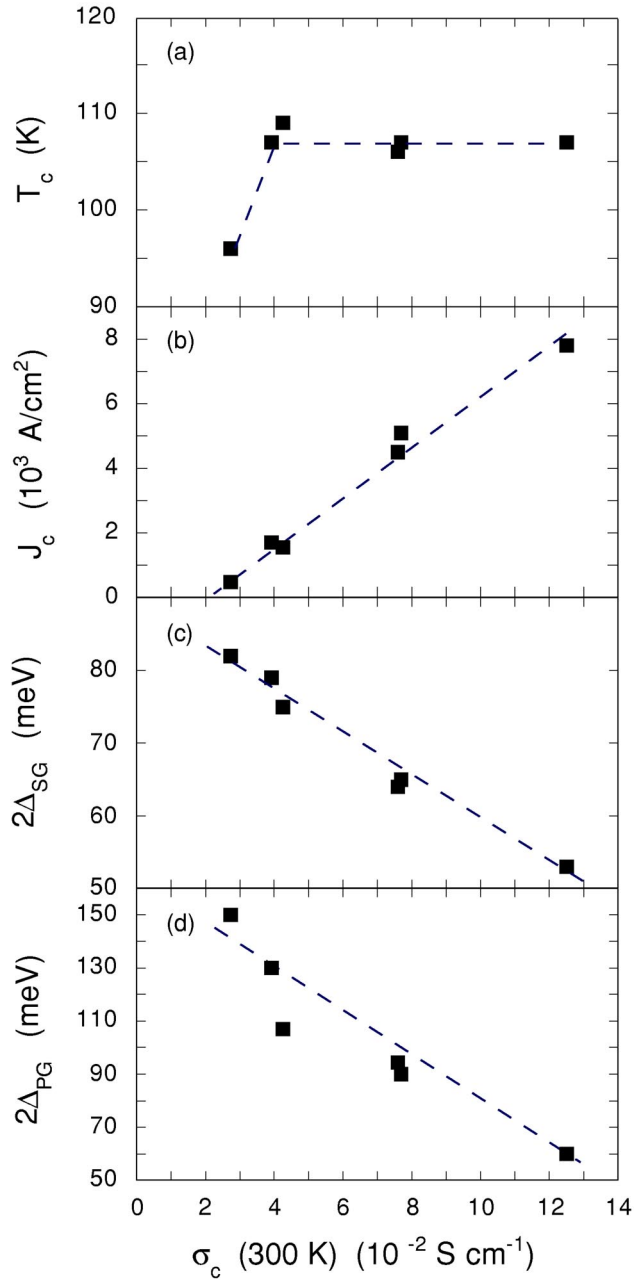


FIG. 7. Plots of T_c , J_c , $2\Delta_{\text{SG}}$, and $2\Delta_{\text{PG}}$ for Bi2223 as a function of $\sigma_c(300\text{ K})$ for samples at various doping levels. Since $\sigma_c(300\text{ K})$ is considered to be roughly proportional to the doping level, the above plots represent the doping dependence for T_c , J_c , $2\Delta_{\text{SG}}$, and $2\Delta_{\text{PG}}$. The dashed lines are guides to the eyes.

$2\Delta_{\text{PG}}$ for samples of different doping levels as a function of $\sigma_c(300\text{ K}) = \rho_c(300\text{ K})^{-1}$, the c -axis conductivity at 300 K. In this figure, the plots include the data for samples which are not listed in Table I. Since the doping level is difficult to determine in the present case, we take $\sigma_c(300\text{ K})$ as a measure of the doping level. This is well substantiated by the transport study conducted by Fujii *et al.*^{27,28} for this Bi2223 system. In Fig. 7, it is clearly recognized that T_c remains unchanged in the overdoped region while $\sigma_c(300\text{ K})$ is increased, or, equivalently, doping is increased. This is the same result as obtained by Fujii *et al.*^{27,28}

On the other hand, J_c shows a tendency to increase almost linearly with increasing doping. As mentioned earlier, this is in accordance with the doping dependence of the superconducting peak height, i.e., $\sigma_T \equiv dI/dV$ at $V = 2\Delta_{\text{SG}}/e$. In ARPES experiments, a similar behavior was observed in the superconducting peak height of the spectral function in Bi2212.^{47,48} Since J_c in a tunnel Josephson junction is proportional to the square root of the superfluid density,⁴⁹ this implies that the superconducting order parameter should increase with increasing doping in the conventional BCS theory. However, this contradicts with the actual observation that Δ_{SG} decreases with increasing doping level. We argue the reason for this inconsistency in the following section.

There is a clear tendency that $2\Delta_{\text{SG}}$ and $2\Delta_{\text{PG}}$ decrease with increasing doping. The behavior is in basic agreement with an expected behavior from the generic phase diagram. In the BCS theory in the weak-coupling limit, the superconducting gap is proportional to T_c . Since the superconductivity behavior in the overdoped region is considered in most cases to be consistent with the BCS behavior,²⁹ the present relationship between the pinned T_c and the decreasing Δ_{SG} is anomalous in this sense. We discuss the reason for this apparently anomalous behavior in the following section with relevance to the inequivalent doping.^{27,28,50}

IV. DISCUSSION

A. Superconducting gap and pseudogap

By the ITS measurements, it has become clear that, in the Bi2223 system, the superconducting gap and the pseudogap exist in a similar way as they do in the Bi2212 system. The magnitude for the superconducting gap of $2\Delta_{\text{SG}} \approx 80\text{ meV}$ for the optimum doping level is similar to or a little larger by no more than 10% than that for the Bi2212 system. In this sense, the scaling between T_c and Δ_{SG} is not as clear as in the case of the ARPES results.^{30,31}

As was previously reported,^{27,28} T_c in the Bi2223 system remains unchanged while the doping level increases from the optimum level, which is at variance with the generic phase diagram.²⁹ The present study has made it clear that Δ_{SG} decreases with increasing doping level while T_c remains unchanged. As mentioned above, this is anomalous if the BCS theory is simply applied. This apparently anomalous behavior can be interpreted in terms of the inequivalent doping model.^{27,28,50} In the Bi2223 system, there are two inequivalent CuO_2 layers, i.e., inner and outer CuO_2 planes. In the inequivalent doping model, the doping level becomes out of balance between these two inequivalent CuO_2 planes; namely, in the overdoped region, the outer CuO_2 planes are more doped and inner CuO_2 planes are less doped. Then it occurs that the doping level of the inner CuO_2 planes are fixed at a value near the optimum level and T_c remains unchanged while the outer CuO_2 planes are overdoped. Since T_c of the system is determined by the higher T_c of the two planes, this results in a pinned T_c of 107 K in the overdoped region.

From the point of view of the proximity effect, this situation is interpreted in terms of McMillan's tunneling model

for the proximity effect.³⁸ Within this framework, it is understood that the inner and outer CuO_2 planes are coupled via tunneling. For such a combination, McMillan's tunneling model predicts that the CuO_2 proximity sandwich has a T_c of the inner plane, which is higher than the other, and an intermediate Δ_{SG} value, which lies between those of the inner and outer CuO_2 planes.^{51,52} When the coupling is weak, the pair potential Δ has two peaks, while when it is strong Δ has only a single peak. In the present case, the coupling is likely to be sufficiently strong, which is consistent with measured σ_T having a single peak at $2\Delta_{\text{SG}}$. The magnitude of Δ_{SG} depends on the coupling strength between these planes.^{51,52} In the present case, the outer CuO_2 planes are overdoped and its Δ_{SG} is much smaller than that at the optimum doping level. Then, from McMillan's tunneling model, the Δ_{SG} value to be observed is smaller than that of the inner plane in the presence of an appropriate coupling strength. Since further doping reduces Δ_{SG} of the outer plane further, it follows that Δ_{SG} decreases with doping, while T_c remains unchanged. The inner plane is thought to play a role of sustaining T_c at its maximum. Thus, the present results for the doping dependence of T_c and Δ_{SG} are reasonably interpreted in terms of McMillan's tunneling proximity model. This also implies that the present result is consistent with the inequivalent doping model in the Bi2223 system.

The present results for Δ_{SG} should be compared with the ARPES results by Feng *et al.*³⁰ and Sato *et al.*³¹ The value of Δ_{SG} for the optimum doping in the present study is 40 meV, which is smaller by ≈ 10 meV than that estimated by the ARPES SCP position and larger by ≈ 10 meV than that estimated by the LEM of the ARPES spectral function. It is known that the SCP position is fixed against T while the LEM decreases with increasing T , which means that the half-width of SCP increases with T (Ref. 53). In contrast, Δ_{SG} obtained by short-pulse ITS clearly decreases with T , the behavior of which is definitely different from the ARPES results. Furthermore, it was reported that the broad ARPES quasiparticle peak at ≈ 50 meV, which is regarded as the pseudogap peak, connects with the SCP below T_c at the same binding energy.³¹ This behavior is also different from the present ITS results, in which no smooth connection is observed between the superconducting gap and the pseudogap. The present results are in agreement with the ARPES results only in that both gap structures exist. The behavior and the magnitude of both gap structures are different between the two spectroscopy results in the strict meaning. As for the value for T^* , Sato *et al.*³¹ estimated that $T^* \approx 150$ K. This value is smaller than the transport result^{27,28} or the present tunneling result, in which a finer resolution is attained.

B. Peak-dip-hump structure

The PDH structure is commonly observed in the energy spectrum for high- T_c superconductors in various spectroscopic experiments. In the present study, the PDH structure is more clearly observed than in other observations because of SIS tunneling. The cause of the PDH structure is supposed variously. The most straightforward one is the existence of another peak structure in the single-particle excitation den-

sity of states (DOS) above the superconducting peak, say, at $E = \Omega$. In this case, a SIS tunneling spectrum exhibits three peaks at $V = 2\Delta/e$, $(\Delta + \Omega)/e$, and $2\Omega/e$. When the DOS peak at $E = \Omega$ is broad, the SIS tunneling conductance peak at $V = 2\Omega/e$ becomes almost indiscernible, as simple numerical calculations show, and the peak at $V = (\Delta + \Omega)/e$ can be quite sharp, forming a clear PDH structure reminiscent of the spectra shown in Fig. 5. If we regard the hump as a peak arising from such a broad DOS peak at $E = \Omega$, the values for Ω are determined from Fig. 5. It is found that Ω decreases with increasing T , as is seen from the T -dependent hump position shown in Fig. 6. The rate of decrease is slightly faster than that of Δ for underdoped sample A and more or less slower for overdoped sample C. For sample B, the temperature dependence of Ω nearly scales with that of Δ . The values for Ω at 10 K are 79, 76, and 50 meV for samples A, B, and C, respectively, showing a tendency to decrease with increasing doping level. At present, we know nothing definite about such a single-particle excitation peak in the DOS but the superconducting peak. However, it may be interesting to note that the broad pseudogap peak, which can be distinct from the superconducting peak below T_c , might lead to the broad DOS peak. In this sense, it should be noted that the background in the tunneling spectrum clearly exhibits a significant T dependence below T_c . This might be linked with a systematic T dependent change in the growth of the conductance background above T_c , which is a pseudogap and which smoothly changes to the broad hump structure below T_c .

The present values for the dip and hump positions for Bi2223 ITS spectrum are 80–100 meV and 100–120 meV, respectively. Strikingly, these values are compared with the Bi2212 break junction results of 70–90 meV for the dip position and 100–140 meV for the hump position.^{32,34,46,54} There are only a few reports on Bi2223 break junctions,^{55,56} in which the peak and dip were observed to be located at 80–105 meV and ~ 170 meV, respectively. Clearly, the latter is much greater than the present observations. The reason of this discrepancy has yet to be known.

On the other hand, the PDH structure is also observed in the superconductor/insulator/normal-metal (SIN) tunneling spectroscopy. For example, the dip position in the STS spectrum for the Bi2212 system ranges from 70 to 90 meV and the hump position ranges from 100 to 150 meV.^{3,14} These values are rather common in SIN tunneling spectroscopy.^{34,57} From these values, it follows that $\Omega = 100$ –150 meV and the hump position for SIS tunneling to be compared should be 130–190 meV, provided $\Delta_{\text{SG}} = 30$ –40 meV. These values are larger than the hump position values of 100–140 meV obtained from Bi2212 break junctions.^{34,54,57} They are also larger than the hump position values of 80–120 meV for the Bi2223 ITS tunneling results in the present study. Although there is some quantitative discrepancy in the values for Ω , it does not seem to rule out the possibility that the PDH structure arises from the broad DOS peak.

It was argued that the dip-peak separation scales with T_c and reaches the maximum when the doping is optimum.³² In the present results, a similar tendency is seen as far as the optimum and overdoped samples are concerned. In the un-

derdoped region, however, the dip-peak separation of 23.3 meV at 10 K is larger than that of 21.6 meV at the optimum doping or that of 16.5 meV in the overdoped region, as seen in Fig. 5, presenting a conflicting tendency. Thus, in the Bi2223 system, it is difficult to find a simple correlation between PDH structure and T_c as argued by Zasadzinski *et al.*³² for the Bi2212 system. Rather, the present result simply displays a clear tendency that the PDH structure is enhanced as the doping decreases. Furthermore, it should be noted that the peak-dip separation shown in Fig. 5 decreases with increasing T . In some models, this separation energy is associated with the neutron resonance peak energy.³² However, the neutron resonance peak energy is actually nearly constant below T_c (Ref. 58) and increases with increasing T (Ref. 59), the behavior of which is at variance with the present results.

The PDH structure is more commonly observed in the ARPES spectra near $(\pi, 0)$ position both in the Bi2212 and the Bi2223 system.^{30,31} Recently, it is proposed that this PDH structure is caused by the bilayer splitting,³³ in which the sharp quasiparticle peak is attributed to the antibonding band and the broad hump to the bonding band. The bilayer splitting was actually observed near $(\pi, 0)$ in the Bi2212 system.^{53,60} However, it appears that the energy splitting is not seen in the recent ARPES experiments on Bi2223 system.^{30,31} In cuprate superconductors, the c -axis hopping integral is proportional to $(\cos k_x - \cos k_y)^2$ (Ref. 61), so that the tunneling conductance spectrum reflects an ARPES spectral function with a large weight in the $(\pi, 0)$ direction. Therefore, the tunneling spectrum and the ARPES result should have a correlation with respect to the PDH structure. In this sense, the hump position in the ARPES spectrum reflects the value for Ω (150 meV [Ref. 31], 120 meV [Ref. 30]). Clearly, these values are nearly equal to those in SIN tunneling spectra, and a similar argument applies to this case. Also in this case, the PDH results in the ARPES observation presents a similar quantitative discrepancy, which remains to be known.

It is argued in some models^{32,36,37} that this dip is a signature of strong coupling to an excitation of some kind, say, magnetic origin. However, as mentioned above, it is difficult to find evidence which directly relates this dip to an excitation that is supposed to be involved in the pairing of quasiparticles. We should rather say at this point that the PDH structure clearly indicates the transfer of quasiparticle density of states from the dip position to the superconducting peak when the system undergoes the transition.

C. Maximum Josephson current and the normal-state tunneling resistance

In the BCS theory, the maximum Josephson current I_c is expressed as⁴⁹

$$I_c = \frac{\pi \Delta_{SG}}{2eR_N} \tanh \frac{\Delta_{SG}}{2k_B T}. \quad (1)$$

Therefore, I_c is proportional to the superconducting order parameter Δ_{SG} at low temperatures. In this framework, it should follow that the maximum Josephson current density

J_c gradually decreases with increasing doping because Δ_{SG} decreases concomitantly. However, this is not the case, as seen in Fig. 7. The present results indicate the opposite tendency for J_c ; namely, J_c increases with increasing doping in spite of a decrease in Δ_{SG} . Similar behavior was also observed in the Bi2212 system.⁶² It is rather likely that this behavior of J_c is generally seen in cuprates.

Equation (1) may indicate that the increase in J_c shown in Fig. 7(b) is simply caused by a decrease in the normal-state tunneling resistance R_N . However, a change in R_N , namely, an increase in $\sigma_c(300 \text{ K})$ from the lowest to the highest for the samples in Fig. 7, is insufficient to explain the increase in J_c . When $\sigma_c(300 \text{ K})$ increases 4.7 times from 0.027 to 0.125 S cm^{-1} in Fig. 7, R_N decreases 0.21 times, since R_N is thought to be proportional to $\rho_c(300 \text{ K})$, as conjectured from Fig. 4. From Fig. 7(c), Δ_{SG} decreases by a factor of 0.65. With these values, the increase in J_c is calculated from Eq. (1) to be a factor of 3.1. Clearly, this value is smaller than that for the increase in J_c of a factor of ~ 15 . Therefore, it is evidently difficult to explain the increase in J_c with doping solely in terms of a simple ordinary picture. Similar behavior is observed also in the Bi2212 system.^{62,63} The fact that J_c increases significantly while Δ_{SG} decreases is indeed extraordinary in light of the conventional superconductivity model. It seems that this behavior conveys an important implication concerning the nature of high- T_c superconductivity or at least in the Bi2223 and the Bi2212 system.

This apparently contradictory behavior of J_c can be interpreted reasonably and uniquely only when the junction electrodes, i.e., the CuO_2 planes in the present case, consist of superconducting regions and nonsuperconducting highly resistive regions. In the latter regions, we assume rather depleted density of states so that the tunneling conductivity is small. In this model, it is reasonably assumed that an increase in the doping level leads to an increase in the superconducting area, or the superconducting fraction f_S of the electrode, while the area-normalized tunneling probability and the density of states in each area are supposed not to change significantly. When the superconductor is phase separated in such a way, the Josephson current flows only in junction portions where both sides are in the superconducting phase. From this it follows that $J_c \propto f_S^2$. This contrasts sharply with the case in which the superconductor is homogeneous, or superconducting regions are located in correlated positions on both sides of the junction and $J_c \propto f_S$. To evaluate the change in f_S , we use an approximate relationship $f_S \propto \sigma_c(300 \text{ K})$ (Ref. 64), from which it follows that f_S increases 4.7 times in the same doping range. Combining Eq. (1), $J_c \propto \Delta_{SG} f_S^2$, from which J_c turns out to increase 14.4 times. Clearly, this value is in good agreement with the observed value of ~ 15 . This experimental result provides evidence for the phase-separated superconductivity in this system.

The implication of this consequence is decisively important. The result strongly suggests that the phase separation takes place in the Bi2223 system and that the fraction of the superconducting phase increases with doping. This is also probably the case in the Bi2212 system for the same reason.

This consequence is consistent with the recent STS observation of inhomogeneous distribution of the superconducting order parameter.^{17,18,65} By inhomogeneity, however, we should mean spatial distribution of superconducting regions, since the systematic change in the tunneling conductance and the sharpness of its superconducting peak imply that the magnitude of the order parameter is regarded rather homogeneous in the superconducting region.

V. CONCLUSION

Using the short-pulse ITS, we have measured the superconducting gap and the pseudogap for the CuO₂ triple-layer Bi₂Sr₂Ca₂Cu₃O_{10+ δ} system. It is found that the magnitude of the superconducting gap and the pseudogap are ≈ 80 meV and 130 meV, respectively, in the case of optimum doping. Together with these gap structures, a clear dip-and-hump structure is observed. The energy scales for these gap structures decrease with increasing doping level, showing a similar tendency observed for the CuO₂ double-layer system. In

the overdoped region, the superconducting gap is observed to decrease with increasing doping while T_c remains unchanged. This fact is interpreted in terms of McMillan's tunneling proximity model. It is found that the peak-dip-hump structure observed in the tunneling spectrum does not necessarily correspond straightforwardly to that of the ARPES results. It is found that the decrease in the superconducting gap and the increase in the maximum Josephson current with increasing doping imply that the phase separation takes place between superconducting region and nonsuperconducting highly resistive region.

Note added. After the submission of this manuscript, we noted a paper reporting a doping dependent Δ_{SG} for the Bi2223 system based on ARPES experiments.⁶⁶

ACKNOWLEDGMENT

This work was partially supported by The Mitsubishi Foundation.

*Present address: Department of Applied Physics, School of Science and Engineering, Waseda University, Tokyo 169-8555, Japan.

[†]Present address: NTT Photonics Laboratories, 3-1 Morinosato-Wakamiya, Atsugi, Kanagawa 243-0198, Japan.

[‡]Corresponding author. Electronic address: suzuki@kuee.kyoto-u.ac.jp

¹E.L. Wolf, *Principles of Electron Tunneling Spectroscopy* (Oxford University Press, Oxford, 1985).

²J.G. Bednortz and K.A. Müller, *Z. Phys. B: Condens. Matter* **64**, 189 (1986).

³C. Renner and Ø. Fischer, *Phys. Rev. B* **51**, 9208 (1995).

⁴C. Renner, B. Revaz, J.Y. Genoud, K. Kadowaki, and Ø. Fischer, *Phys. Rev. Lett.* **80**, 149 (1998).

⁵M. Suzuki, S. Karimoto, and K. Namekawa, *J. Phys. Soc. Jpn.* **67**, 732 (1998).

⁶M. Suzuki, T. Watanabe, and A. Matsuda, *Phys. Rev. Lett.* **82**, 5361 (1999).

⁷G. Binnig, H. Rohrer, C. Gerber, and E. Weibel, *Appl. Phys. Lett.* **40**, 178 (1982).

⁸R. Kleiner, F. Seimeyer, G. Kunkel, and P. Müller, *Phys. Rev. Lett.* **68**, 2394 (1992).

⁹R. Kleiner and P. Müller, *Phys. Rev. B* **49**, 1327 (1994).

¹⁰H.F. Hess, R.C. Dynes, J.J.M. Valles, and J.V. Waszczak, *Phys. Rev. Lett.* **62**, 214 (1989).

¹¹H.F. Hess, R.B. Robinson, and J.V. Waszczak, *Phys. Rev. Lett.* **64**, 2711 (1990).

¹²M. Kugler, Ø. Fischer, C. Renner, S. Ono, and Y. Ando, *Phys. Rev. Lett.* **86**, 4911 (2001).

¹³S. Kaneko, N. Nishida, K. Mochiku, and K. Kadowaki, *Physica C* **298**, 105 (1998).

¹⁴A. Matsuda, S. Sugita, and T. Watanabe, *Phys. Rev. B* **60**, 1377 (1999).

¹⁵M. Oda, C. Manabe, and M. Ido, *Phys. Rev. B* **53**, 2253 (1996).

¹⁶C. Renner, B. Revaz, K. Kadowaki, I. Maggio-Aprile, and Ø. Fischer, *Phys. Rev. Lett.* **80**, 3606 (1998).

¹⁷A. Matsuda, 2001 Annual Meeting of the Physical Society of

Japan, Extended Abstract, 17aTE5, 17aTE6.

¹⁸K.M. Lang, V. Madhavan, J.E. Hoffman, E.W. Hudson, H. Eisaki, S. Uchida, and J.C. Davis, *Nature (London)* **415**, 412 (2002).

¹⁹J.E. Hoffman, E.W. Hudson, K.M. Lang, V. Madhavan, H. Eisaki, S. Uchida, and J.C. Davis, *Science* **295**, 466 (2002).

²⁰C. Howald, H. Eisaki, N. Kaneko, and A. Kapitulnik, *cond-mat/0205118* (unpublished).

²¹M. Suzuki and T. Watanabe, *Phys. Rev. Lett.* **85**, 4787 (2000).

²²V.M. Krasnov, A. Yurgens, D. Winkler, P. Delsing, and T. Claeson, *Phys. Rev. Lett.* **84**, 5860 (2000).

²³V.M. Krasnov, A.E. Kovalev, A. Yurgens, and D. Winkler, *Phys. Rev. Lett.* **86**, 2657 (2001).

²⁴A. Yurgens, D. Winkler, T. Claeson, S.J. Hwang, and J.H. Choy, *Int. J. Mod. Phys. B* **13**, 3758 (1999).

²⁵K. Schlenga, R. Kleiner, G. Hechtfisher, M. Möble, S. Schmitt, P. Müller, Ch. Helm, Ch. Preis, F. Forsthofer, J. Keller, H.L. Johnson, M. Veith, and E. Steinbeiß, *Phys. Rev. B* **57**, 14 518 (1998).

²⁶T. Fujii, T. Watanabe, and A. Matsuda, *J. Cryst. Growth* **223**, 175 (2001).

²⁷T. Fujii, T. Watanabe, and A. Matsuda, *Physica C* **357-360**, 173 (2001).

²⁸T. Fujii, I. Terasaki, T. Watanabe, and A. Matsuda, *Phys. Rev. B* **66**, 024507 (2002).

²⁹J.L. Tallon, C. Bernhard, H. Shaked, R.L. Hitterman, and J.D. Jorgensen, *Phys. Rev. B* **51**, 12 911 (1995).

³⁰D.L. Feng, A. Damascelli, K.M. Shen, N. Motoyama, D.H. Lu, H. Eisaki, K. Shimizu, J.-i. Shimoyama, K. Kishio, N. Kaneko, M. Greven, G.D. Gu, X.J. Zhou, C. Kim, F. Ronning, N.P. Armitage, and Z.-X. Shen, *Phys. Rev. Lett.* **88**, 107001 (2002).

³¹T. Sato, H. Matsui, S. Nishina, T. Takahashi, T. Fujii, T. Watanabe, and A. Matsuda, *Phys. Rev. Lett.* **89**, 067005 (2002).

³²J.F. Zasadzinski, L. Ozyuzer, N. Miyakawa, K.E. Gray, D.G. Hinks, and C. Kendziora, *Phys. Rev. Lett.* **87**, 067005 (2001).

³³A.A. Kordyuk, S.V. Borisenko, T.K. Kim, K. Nenkov, M. Knupfer, M.S. Golden, J. Fink, H. Berger, and R. Follath, *Phys. Rev. Lett.* **89**, 077003 (2002).

- ³⁴Y. DeWilde, N. Miyakawa, P. Guptasarma, M. Iavarone, L. Ozyuzer, J.F. Zasadzinski, P. Romano, D.G. Hinks, C. Kendziora, G.W. Crabtree, and K.E. Gray, Phys. Rev. Lett. **80**, 153 (1998).
- ³⁵D. Coffey and L. Coffey, Phys. Rev. Lett. **70**, 1529 (1993).
- ³⁶A. Abanov and A.V. Chubukov, Phys. Rev. Lett. **83**, 1652 (1999).
- ³⁷J. Mesot, M. Boehm, M.R. Norman, M. Randeria, N. Metoki, A. Kaminski, S. Rosenkranz, A. Hiess, H.M. Fretwell, J.C. Campuzano, and K. Kadowaki, cond-mat/0102339 (unpublished).
- ³⁸W.L. McMillan, Phys. Rev. **175**, 537 (1968).
- ³⁹V.M. Krasnov, A. Yurgens, D. Winkler, and P. Delsing, J. Appl. Phys. **89**, 5578 (2001).
- ⁴⁰S. Kojima, Graduation thesis, Kyoto University, 2001.
- ⁴¹T. Watanabe, T. Fujii, and A. Matsuda (unpublished).
- ⁴²T. Hamatani, K. Anagawa, T. Watanabe, and M. Suzuki, Physica C **390**, 89 (2003).
- ⁴³T. Watanabe, T. Fujii, and A. Matsuda, Phys. Rev. Lett. **79**, 2113 (1997).
- ⁴⁴The ρ_c values for the mesa samples are two to three times larger than those obtained from bulk single crystals (Ref. 28). A possible cause might be dislocation lines in the ab planes, which function to shortcut the interplanes in large size crystals. For small mesa samples as in the present study, it is thought to be rare that a dislocation line penetrate a mesa which has such a small cross section.
- ⁴⁵In the case where a single Bi2212 intergrowth layer is included in a mesa which has ten junctions, two junctions out of ten are heterojunctions. With Δ_1 and Δ_2 being the gap magnitudes for Bi2212 and Bi2223, respectively, the heterojunction has a conductance peak at $\Delta_1 + \Delta_2$, and the other junctions have a peak at $2\Delta_2$. Since series characteristics are measured, the total gap magnitude is $18\Delta_2 + 2\Delta_1$. If we assume that $\Delta_1 = \Delta_2(1 - \epsilon)$, where $\epsilon \leq 0.2$, then $10\Delta_{pp} = 20\Delta_2(1 - 2/20\epsilon) = 20\Delta_2(1 - 0.02)$. Therefore, the error due to a single Bi2212 intergrowth layer is estimated to be a few percent or less.
- ⁴⁶N. Miyakawa, P. Guptasarma, J.F. Zasadzinski, D.G. Hinks, and K.E. Gray, Phys. Rev. Lett. **80**, 157 (1998).
- ⁴⁷D.L. Feng, D.H. Lu, K.M. Shen, C. Kim, H. Eisaki, A. Damascelli, R. Yoshizaki, J.-i. Shimoyama, K. Kishio, G.D. Gu, S. Oh, A. Andrus, J. O'Donnell, J.N. Eckstein, and Z.-H. Shen, Science **289**, 277 (2000).
- ⁴⁸H. Ding, J.R. Engelbrecht, Z. Wang, J.C. Campuzano, S.C. Wang, H.B. Yang, R. Rogan, T. Takahashi, K. Kadowaki, and D.G. Hinks, Phys. Rev. Lett. **87**, 227001 (2001).
- ⁴⁹V. Ambegaokar and A. Baratoff, Phys. Rev. Lett. **10**, 486 (1963); **11**, 104 (1963).
- ⁵⁰S.A. Kivelson, Physica B **318**, 61 (2002).
- ⁵¹J. Vrba and S.B. Woods, Phys. Rev. B **3**, 2243 (1971).
- ⁵²V. Keith and J.D. Leslie, Phys. Rev. B **18**, 4729 (1978).
- ⁵³D.L. Feng, N.P. Armitage, D.H. Lu, A. Damascelli, J.P. Hu, P. Bogdanov, A. Lanzara, F. Ronning, K.M. Shen, H. Eisaki, C. Kim, Z.-X. Shen, J.-i. Shimoyama, and K. Kishio, Phys. Rev. Lett. **86**, 5550 (2001).
- ⁵⁴D. Mandrus, J. Hartge, C. Kendziora, L. Mihaly, and L. Forro, Europhys. Lett. **22**, 199 (1993).
- ⁵⁵T. Ekino, S. Hashimoto, T. Takasaki, and H. Fujii, Phys. Rev. B **64**, 092510 (2001).
- ⁵⁶S.I. Vedenev and V.A. Stepanov, Pis'ma Zh. Eksp. Teor. Fiz. **73**, 159 (2001) [JETP Lett. **73**, 141 (2001)].
- ⁵⁷N. Miyakawa, J.F. Zasadzinski, L. Ozyuzer, P. Guptasarma, D.G. Hinks, C. Kendziora, and K.E. Gray, Phys. Rev. Lett. **83**, 1018 (1999).
- ⁵⁸P. Dai, H.A. Mook, S.M. Hayden, G. Aeppli, T.G. Perring, R.D. Hunt, and F. Doğan, Science **284**, 1344 (1999).
- ⁵⁹H.F. Fong, B. Keimer, D. Reznik, D.L. Milius, and I.A. Aksay, Phys. Rev. B **54**, 6708 (1996).
- ⁶⁰Y.-D. Chuang, A.D. Gromko, A. Fedorov, Y. Aiura, K. Oka, Y. Ando, H. Eisaki, S. Uchida, and D.S. Dessau, Phys. Rev. Lett. **87**, 117002 (2001).
- ⁶¹T. Xiang and J.M. Wheatley, Phys. Rev. Lett. **77**, 4632 (1996).
- ⁶²M. Suzuki and S. Karimoto, IEICE Trans. Electron. **E81-C**, 1518 (1998).
- ⁶³M. Suzuki, T. Watanabe, and A. Matsuda, IEEE Trans. Appl. Supercond. **9**, 4511 (1999).
- ⁶⁴In this model, the c -axis conductivity σ_c is a function of the CuO₂ double-layer sheet conductivity σ_{sh} and tunneling conductivities σ_{ss} , σ_{sn} , and σ_{nn} , where σ_{ss} denotes the tunneling conductivity between superconductive regions, σ_{sn} denotes the one between superconductive and nonsuperconductive regions, and σ_{nn} between nonsuperconductive regions. If we neglect σ_{sh} , $\sigma_c = \sigma_{ss}f_S^2 + 2\sigma_{sn}f_S(1-f_S) + \sigma_{nn}(1-f_S)^2 = \sigma_{nn} + 2(\sigma_{sn} - \sigma_{nn})f_S + (\sigma_{ss} + \sigma_{nn} - 2\sigma_{sn})f_S^2$. It is probable that $\sigma_{ss} \gg \sigma_{sn} \gg \sigma_{nn}$. Then $\sigma_c \approx \sigma_{nn} + 2\sigma_{sn}f_S + \sigma_{ss}f_S^2$. Under this condition and in an appropriate range for $f_S \leq 0.5$, we have an approximate relationship that $\sigma_c \sim \sigma' f_S$ with an appropriate constant for σ' . Since this relationship is used to evaluate the change in f_S from σ_c , this approximation works sufficiently.
- ⁶⁵S.H. Pan, J.P. O'Neal, R.L. Badzey, C. Chamon, H. Ding, J.R. Engelbrecht, Z. Wang, H. Eisaki, S. Uchida, A.K. Gupta, K.-W. Ng, E.W. Hudson, K.M. Lang, and J.C. Davis, Nature (London) **413**, 282 (2001).
- ⁶⁶H. Matsui, T. Sato, T. Takahashi, H. Ding, H.-B. Yang, S.-C. Wang, T. Fujii, T. Watanabe, A. Matsuda, T. Terashima, and K. Kadowaki, Phys. Rev. B **67**, 060501 (2003).